Molecular Dynamics Studies of the Structural Change in 1,3-Diamino-2,4,6-trinitrobenzene (DATB) in the Crystalline State under High Pressure

Yuji Kohno,*,† Reiko I. Hiyoshi,*,§ Yoshitaka Yamaguchi,† Shinya Matsumoto,‡ Atsushi Koseki,‡ Osamu Takahashi,|| Katsuyoshi Yamasaki,|| and Kazuyoshi Ueda†

Department of Materials Chemistry, Graduate School of Engineering, Yokohama National University, Tokiwadai 79-5, Hodogaya-ku, Yokohama 240-8501, Japan, Department of Environment and Natural Sciences, Graduate School of Environment and Information Sciences, Yokohama National University, Tokiwadai 79-2, Hodogaya-ku, Yokohama 240-8501, Japan, Explosion Investigation Section, National Research Institute of Police Science, Kashiwanoha 6-3-1, Kashiwa 277-0882, Japan, and Department of Chemistry, Graduate School of Science, Hiroshima University, Kagamiyama 1-3-1, Higashi-Hiroshima 739-8526, Japan

Received: October 19, 2008; Revised Manuscript Received: January 13, 2009

Molecular dynamics (MD) calculations were performed to reveal the effect of high pressure on the crystal of 1,3-diamino-2,4,6-trinitrobenzene (DATB). The coordinates of the individual atoms in the DATB crystal structure were obtained using X-ray diffraction analysis. The primary simulation cell consists of 54 molecules in a monoclinic cell, corresponding to 27 unit cells obtained by replicating the experimentally determined unit cell. The pressure dependence of intermolecular distance concerning hydrogen bonds in the DATB crystal was investigated in the range of 1 atm to 25.0 GPa by increasing the pressure at every 0.5 GPa. Intermolecular distances of the hydrogen bonds between the nitro and amino groups decrease with increasing pressure up to 25.0 GPa, except in the range of 7.5 to 8.5 GPa. A unique structural change in the DATB crystal occurred at ~7.5 GPa. Intermolecular distances began to remarkably increase at 7.5 GPa and kept increasing until 8.5 GPa. To clarify the origin of this strange behavior, we used the same pressure regions as those above to analyze the changes in the dihedral angles defined by the plane of the nitro or amino group and by the aromatic rings of hydrogen bonds. The results showed a strong correlation between the increment of the intermolecular distances and the changes in the dihedral angles for these groups. Moreover, when the pressure dependence of the crystal parameter was analyzed, it was found that the *a*-axis length did not change despite the change in the lengths of the other two axes. The direction of the *a* axis corresponds to the direction of intermolecular hydrogen bond networks in the crystal. The results of the present MD calculations explained our previous results for Raman spectra measurements. Further analysis showed that these hydrogen bonds play an important role in stabilizing the energy change of the crystal system.

1. Introduction

The molecular design of new energetic materials with lower sensitivity and higher performance requires an understanding of the complicated mechanisms that underly explosion reactions. However, the details of these processes have not been fully investigated. There are many kinds of aromatic nitro compounds, which are known as energetic materials. Their sensitivities and behaviors vary widely among aromatic nitro derivatives.[1] The physical phenomena involving the pressure and temperature that occur after the detonation process have been reported for related nitro compounds. However, it is technically difficult to measure the in situ phenomena because explosive energy such as that of light, heat, and pressure is enormous. Consequently, the chemical phenomena of the detonation process have remained unclear.

In our previous study,[2] 5-nitro-2,4-dihydro-1,2,4-triazole-3-one (NTO) was investigated by Raman spectroscopy, and the intermolecular interactions by the hydrogen bond showed noteworthy effects on structural change under high-pressure conditions. In general, when the molecule is compressed, the Raman bands exhibit blue shifts due to the decrease in the bond length with increasing pressure. However, the carbonyl stretching in NTO showed a red shift when the pressure was loaded up to ca. 5 GPa. Then, upon further compression, the band moved toward a higher frequency. Molecular dynamics (MD) simulations also indicated that the distance between carbon and oxygen in the carbonyl group increased with pressure up to 10 GPa and decreased upon further increment of the pressure. The change in the bond length between the carbon and oxygen atoms was found to correspond to the change in the Raman band. From these results, we postulated that the above structural change worked as a stabilizer for the stimuli. This change may facilitate the release of strain in the NTO molecule under high-pressure conditions. The intermolecular effect by the hydrogen bond observed in NTO is an important factor in determining the manner in which the reaction paths are created.

On the other hand, 1,3,5-triamino-2,4,6-trinitrobenzene (TATB) (Figure 1a) is known to have a considerably low sensitivity among the nitro aromatic explosives.[3–6] Many reports on molecular structure have discussed the intramolecular or intermolecular hydrogen bond on the basis of the theoretical calculations.[5–17] From these works, the low sensitivity of this molecule has accounted for its high symmetric property such

* Corresponding authors. (Y.K.) Tel: +81-045-339-3945. Fax: +81-045-339-3945. E-mail: kohnoy@ynu.ac.jp. (R.I.H.) Tel: +81-4-7135-8001. Fax: +81-4-7133-9169. E-mail: ichiki@nrips.go.jp.

† Department of Materials Chemistry, Graduate School of Engineering, Yokohama National University.

‡ Department of Environment and Natural Sciences, Graduate School of Environment and Information Sciences, Yokohama National University.

§ National Research Institute of Police Science.

|| Hiroshima University.

10.1021/jp809240x CCC: $40.75
Published on Web 02/20/2009

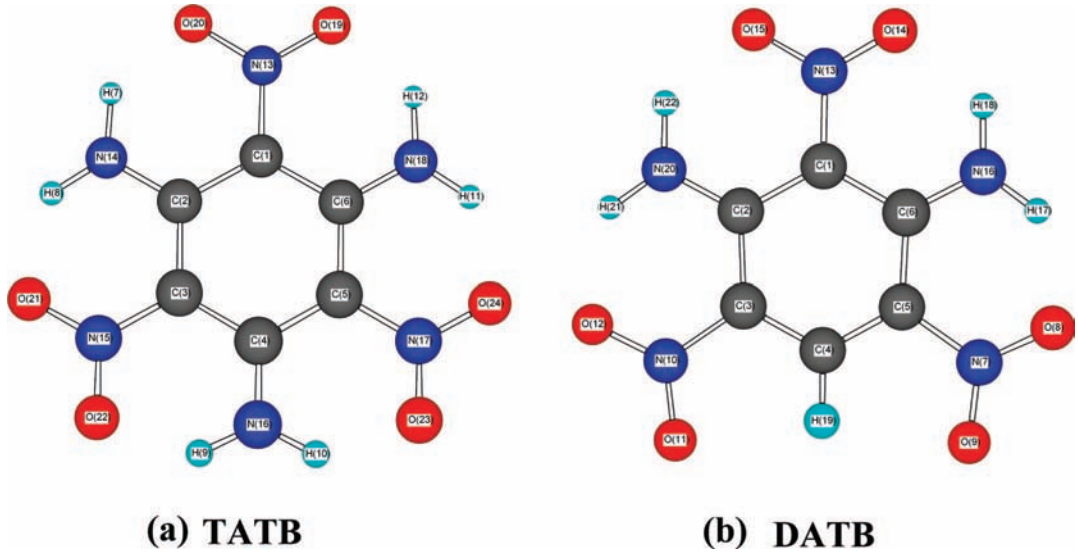

Figure 1. Molecular structures of (a) TATB and (b) DATB. The number on each DATB atom corresponds to the number used in the computational calculation.

as 2D planar networks in the crystalline state where the molecules are aligned in the layered structure. In the crystal, the surfaces of interlayer aromatic rings orient almost in parallel with each other. The shortest distance between the interlayer amino nitrogen and the nitro oxygen is 3.36 Å. In this manner, the TATB molecules form 2D planar networks in the crystalline state. This stable crystal structure of TATB has been considered to be one of the most important factors in insensitivity in energetic materials. Compared with the attention researchers have paid to the TATB molecule, there are few works on the 1,3-diamino-2,4,6-trinitrobenzene (DATB) molecule (Figure 1b) despite the close similarity in chemical structure and the low sensitivity between these two molecules. A DATB molecule also forms a planar conformation because it has two kinds of intramolecular hydrogen bonds between adjacent amino and nitro groups,[18] similar to the TATB molecule. In the crystalline state, DATB molecules do not form 2D planar networks, although they are linked together into a 1D continuous chain by intermolecular hydrogen bonds. Despite such an interesting difference between the structures of the two molecules, there are few studies on the DATB. Indeed no studies have used MD simulations to clarify the dynamic mechanism underlying the initial reaction step of the DATB crystal under high pressure.

In the present work, we carried out MD simulations of the DATB crystal to study the initial decomposition process of the molecules in relation to the intermolecular and intramolecular hydrogen bond under high pressure of up to 25.0 GPa. In particular, we focused on the effect of the DATB geometry in the crystalline state on the stability of the molecule under high-pressure conditions. In the calculation, accurate information on the crystalline state was essential for constructing the initial structure of the simulation cell. The crystal parameters of DATB were determined by Holden in 1967.[18] However, the accuracy of Holden's crystal data was not sufficient for our purpose with the MD simulation because the *R* factor of their DATB data was 10.3%. Although the locations of the hydrogen atoms are important for the elucidation of the structure of the intermolecular and the intramolecular hydrogen bond, they have not been determined. Therefore, a single DATB crystal suitable for X-ray analysis was prepared in this work, and the geometry of DATB in the crystalline state was precisely determined again using single-crystal X-ray diffraction at −50 °C to obtain detailed information in the crystalline state, such as the locations of the hydrogen atoms, sufficient to carry out our MD simulations.

2. Experimental Procedure for X-ray Crystallography

DATB was purchased from Chugoku-kayaku. 1,2-Dichloroethane and *n*-hexane were commercially available and used without further purification. A single DATB crystal of a suitable size was obtained by recrystallization from 1,2-dichloroethane/*n*-hexane at room temperature and was mounted on a glass fiber. All measurements were made on a Rigaku AFC-7R diffractometer with graphite monochromated Mo Kα radiation (λ = 0.71069 Å) and a rotating anode generator. The data collections were carried out at −50 ± 2 °C using the $\omega - 2\theta$ scan technique to a maximum 2θ value of 60.00°. Cell constants and an orientation matrix for data collection were determined from 25 reflections with 2θ angles in the range of 29.55 to 29.96°. Three standard reflections were monitored at every 150 measurements. In the reduction of data, Lorentz and polarization corrections and an empirical absorption correction (Ψ scan) were made.

The structure was solved by direct methods[19] and expanded using Fourier techniques.[20] The nonhydrogen atoms were refined anisotropically. Hydrogen atoms were located from difference Fourier maps and were isotropically refined. All calculations were performed on an SGI INDY computer using the teXsan crystallographic software package (Molecular Structure Corp.).[21]

3. Computational Methods and Procedures

A. Potential Energy Function. MD simulations were performed to investigate the high-pressure effects on the DATB crystal structure using the CHARMM version 29b2 program.[22] Calculations were performed on the DATB crystal at pressures ranging from 1 atm to 20.0 GPa. The CHARMM29 potential energy function is expressed as follows

$$E = E_{\mathrm{b}} + E_{\theta} + E_{\Phi} + E_{\omega} + E_{\mathrm{VDW}} + E_{\mathrm{el}} \qquad (1)$$

where E_{b} is the bond potential, E_{θ} is the bond angle potential, E_{Φ} is the dihedral angle (torsion) potential, E_{ω} is the improper torsions potential, E_{VDW} is the van der Waals interactions, and E_{el} is the electrostatic potential. The formula for each term is represented as

$$E = \sum k_b(l - l_0)^2 + \sum k_\theta(\theta - \theta_0)^2 + \sum k_\Phi[1 + \cos(n_\Phi - \delta)] + \sum k_\omega(\omega - \omega_0)^2 + \sum_{\text{excl}(i,j)=1} \sqrt{\varepsilon_i^* \varepsilon_j^*}\left[\left(\frac{0.5(r_i^* + r_j^*)}{r_{ij}}\right)^{12} - 2\left(\frac{0.5(r_i^* + r_j^*)}{r_{ij}}\right)^{6}\right] \mathrm{SW}(r_{ji}, r_{on}, r_{off}) + \sum_{\text{excl}(i,j)=1} \frac{q_i q_j}{4\pi\varepsilon_0 r_{ji}^2} \mathrm{SW}(r_{ji}, r_{on}, r_{off}) \quad (2)$$

where k_b, k_θ, k_Φ, and k_ω are force constants of the bonds, angles, dihedral angles, and improper dihedral angles, respectively. The first two terms describe the intramolecular interactions of bonded atoms, and the quantities $(l - l_0)$ and $(\theta - \theta_0)$ are the displacements from the equilibrium bond length (l_0) and angle (θ_0), respectively. The torsion energy term is a four-atom term based on the dihedral angle about an axis defined by the middle pair of atoms. The improper torsion term was designed to maintain planarity of certain planar atoms with a quadratic distortion potential. The nonbonded interaction terms are van der Waals interactions and Coulombic interactions between the partial charges on the individual atoms, where r_{ij} is the distance between the atoms i and j in a system, and ε^* and r^* and SW are the well depth, the position of the minimum in the Lennard-Jones potential, and the switching function defined in the original CHARMM22 paper,[22] respectively. The switching distances (r_{on} and r_{off}) were determined according to size of the primary simulation cell. The parameters for the nonbonded interaction terms are those used in the program CHARMM29.

B. Parameterization. In the present work, we developed a CHARMM-type force field for nitro aromatic compounds, such as DATB and TATB, by using density functional theory (DFT) calculations. In particular, because there are no appropriate parameters for the C (aromatic)−NO_2 moiety of DATB in CHARMM29, DFT calculations were performed at the B3LYP/6-31G(d,p) level to determine the harmonic force constants of the internal potential energy terms in the gas phase. We calculated the bond, angle, and dihedral potential energy curves of isolated DATB by changing the bond length, bond angle, and improper angle by minute values around the optimized structure. From these potential energy curves, the force constants k_b, k_θ, and k_ω were evaluated. The force constant for the dihedral angle (k_Φ) was determined by best fitting between the CHARMM and DFT potential energy curves in the range of 0−360°. The equilibrium values of the bond lengths and the bond angles (l_0, θ_0) were determined by full geometry optimization. Partial atomic charges for DATB were calculated for a single isolated molecule with the optimized geometry by using the Merz−Kollman−Singh (MK) scheme.

Ab initio calculations were carried out with the GAUSSIAN 98[23] program package. The basis sets implemented in the program were employed without modification. The DATB geometry was fully optimized without symmetry constraints by the energy gradient methods. All optimized geometries were obtained by using the Becke 3LYP (B3LYP) hybrid density functional with the 6-311++G(2df,2dp) and the 6-31G(d,p). We calculated vibrational frequencies by using the analytical second derivatives at the B3LYP/6-31G(d,p) and B3LYP/6-311++G(2df,2dp) levels. The harmonic vibrational frequencies determined at DFT levels were scaled by 0.9613.[24]

C. Molecular Dynamics. The DATB X-ray analysis data were used in all simulations. The primary simulation cell was constructed from our observed unit cell. All simulations were performed in the NPT ensemble (constant number of molecules, pressure, and temperature). Periodic boundary conditions were enforced by creating images of the atoms in the primary simulation cell. The lattice parameters and atomic coordinates are minimized together before the MD simulation. It should be noted that the crystal symmetry was maintained when the lattice was optimized.

MD simulations were performed by classical mechanics. Initial velocities for all atoms in these systems were selected at random from Boltzmann distribution at 300 K. Newton's equation of motion was then integrated by using a Verlet integrator with a step size of 0.1 fs, and the nonbonded neighbor list was updated every 20 steps. Long-range interactions were cut off between 13.0 and 15.0 Å by using the switching function.

In the initial simulation, the temperature and pressure of the system were set at 300 K and 1 atm, and the position and orientation of the molecules in the unit cell were taken to be identical to those of the experimental structure. After equilibration for 40 ps at 1 atm and 300 K, an analysis run of MD simulation at each 10 ps was sequentially performed from 1 atm to 25.0 GPa by increasing the pressure at every 0.5 GPa. In the simulation, the pressure dependence of the crystal parameters was also investigated.

TABLE 1: Summary of Crystal Data for DATB

empirical formula	$C_6H_5N_5O_6$
formula weight	243.14
crystal color, habit	yellow, plate
crystal size (mm)	0.22 × 0.18 × 0.08
crystal system	monoclinic
space group	*Pc* (no. 7)
lattice parameters	
a (Å)	7.309(3)
b (Å)	5.169(4)
c (Å)	11.583(2)
β (deg)	95.22(2)
V (Å)^3	435.8(4)
Z value	2
D_{calcd} (g cm^{-3})	1.853
F_{000}	248.00
μ(Mo Kα) (cm^{-1})	1.67
no. of reflections measured	1506
no. of independent reflections	1368 (R_{int} = 0.028)
no. of variables	175
reflection/parameter ratio	7.30
residuals: R_1; R_w	0.038; 0.098
no. of reflections to calculate R_1	1187 ($I > 2.0\sigma(I)$)
goodness of fit indicator	1.41
flack parameter	−4.2(8)
maximum peak in final difference map (e Å^{-3})	0.26
minimum peak in final difference map/e (e Å^{-3})	−0.21

4. Results and Discussion

A. X-ray Crystal Structure of DATB. Crystallographic data and the results of the X-ray diffraction measurement are summarized in Table 1. There are two molecules in the unit cell (Figure 2) with a density of 1.830 g/cm^3 (D_{calcd} = 1.853 g/cm^3). The DATB bond lengths and angles are shown in Table 2. The DATB molecule is approximately planar[18] with intramolecular hydrogen bonds between adjacent amino and nitro groups in the DATB molecule, and the nitro groups in the DATB molecule can be classified into two groups, as shown in Figure 3. That is, the nitro group (1) is the group that adjoins two amino groups, and the other (nitro group (2)) is the group that adjoins one amino group and aromatic proton. The intramolecular distances between the nitro oxygen of nitro group (1) and the amino hydrogens are 1.82(2) and 1.79(3) Å, and the corresponding distances for group (2) are 1.88(2) and 1.89(3) Å, respectively. These values are also shown in Figure 3. Moreover,

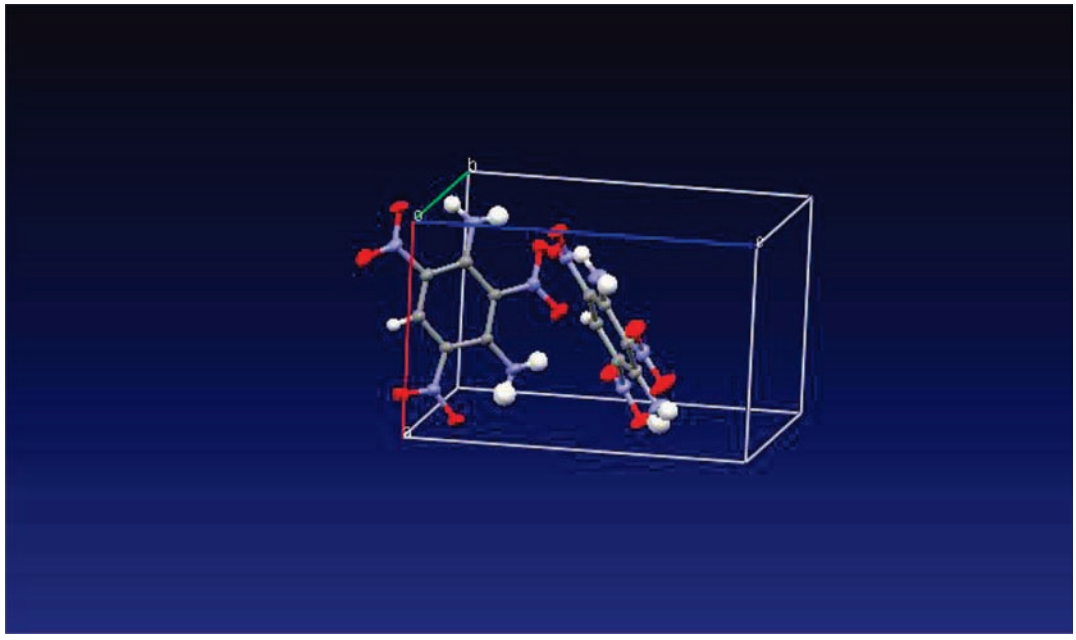

Figure 2. Unit cell of the DATB crystal with thermal ellipsoid drawn at the 50% probability level.[25] Carbon, nitrogen, oxygen, and hydrogen atoms are represented by gray, blue, red, and white, respectively.

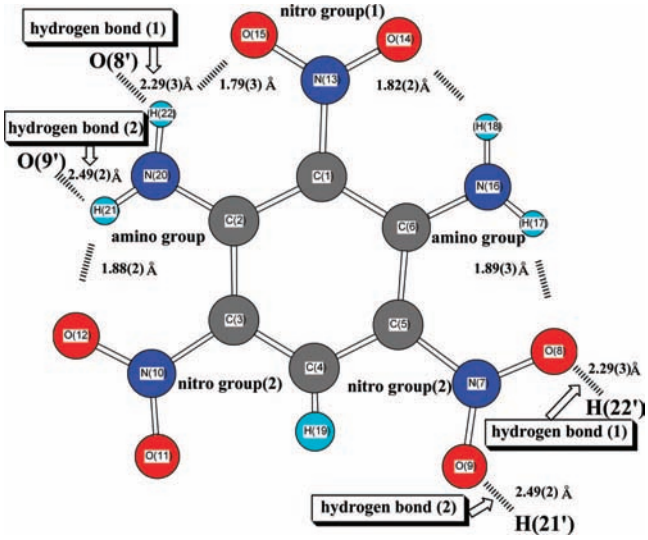

Figure 3. Molecular structure of DATB in the crystalline state.

the DATB molecules are linked to each other by intermolecular hydrogen bonds and form a continuous chain structure along with the *a* axis in the crystal lattice, as shown in Figures 3 and 4. The H(22) and H(21) of the amino group are attached to O(8′) and (O9′) of the nitro group, respectively, of the neighboring molecule located at the next cell. This hydrogen bond linkage forms a linear sheetlike structure. However, DATB molecules do not form 2D planar networks. The intermolecular distances between amino hydrogen and nitro oxygen are 2.29(3) and 2.49(2) Å. The results of X-ray analysis data of DATB were used to build a crystal model in our MD simulations.

B. Optimized Structure and Force Constants of DATB. Table 2 lists the molecular parameters of the optimized structures obtained by the DFT calculations with two different basis sets. The table also shows the experimentally observed values in the crystal. The calculated values with two basis set levels are in good agreement with the experimental data. That is, the conformation of a DATB molecule takes a planar molecule in both cases. The nearest-neighbor hydrogen bond lengths between amino hydrogen H(22) and nitro oxygen O(15) in the nitro group (1) were calculated as 1.770 and 1.765 Å at the B3LYP/6-311++G(2df,2dp) and B3LYP/6-31G(d,p) levels, respectively. These results are also in good agreement with the experimental data. However, the distances between amino hydrogen H(21) and nitro oxygen O(12) in the nitro group (2) were calculated to be 1.801 and 1.795 Å at the B3LYP/6-311++G(2df,2dp) and the B3LYP/6-31G(d,p) levels, which are a little shorter than the observed value of 1.88(2) Å in the crystal. The discrepancy seems to be based on the difference between the hydrogen bond networks formed around groups (1) and (2). Group (1) adjoining two amino groups forms strong hydrogen bond networks among them. Therefore, the electronic structure on the hydrogen bond networks consists of conjugated and delocalized systems. However, group (2) adjoins one amino group and aromatic proton H(19). In this case, the hydrogen bond network formed around group (2) was weak, and the electronic structure was localized. In the crystal, amino hydrogen H(21) was strongly attracted by the electrostatic interaction from nitro oxygen O(9′) in the neighboring molecule. Therefore, the electron density of H(21) in the crystalline state may become lower than that in the gas phase, and the electron cannot be compensated because of the localization of the network on group (2). The low electron density of H(21) may weaken the intramolecular hydrogen bond strength between H(21) and O(12) and would cause an elongation of the intramolecular distance between amino hydrogen H(21) and nitro oxygen O(12) in the nitro group (2) in the crystal state.

Table 3 compares the calculated (B3LYP/6-311++G(2df,2dp) level) and observed vibrational frequencies of DATB crystal. Although the differences were about 50 cm^{-1} in the high-frequency region and the hydrogen bond-related modes, the agreement was generally quite good in all ranges. The order of the vibrational frequencies was also the same when the calculation was performed with a different basis set of the B3LYP/6-31G(d,p) level.

The force constants of DATB are listed in Table 4. The partial atomic charges calculated by the MK method with the B3LYP/6-31G(d,p) level are given in Table 5. The calculated amino

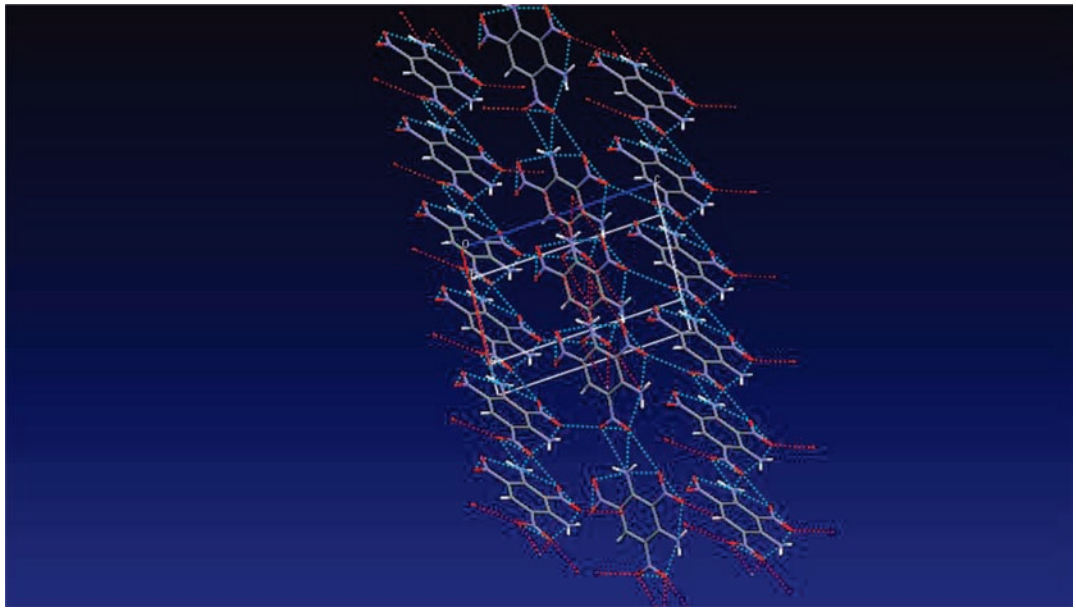

Figure 4. Hydrogen bond structures of DATB in the crystalline state.[25] The DATB molecules are linked by intermolecular hydrogen bonds into continuous chains along with the *a* axis in the crystal lattice. This hydrogen bond linkage forms a sheetlike structure.

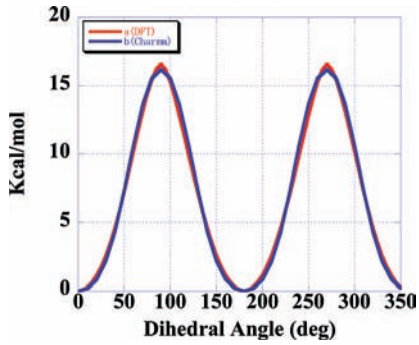

Figure 5. Calculated rotational barrier of nitro group (1) in DATB molecule. (a) DFT calculation at the B3LYP/6-31G(d,p) level. (b) Charmm calculation using eq 2 (the third term) ($n = 2$, $k_\Phi = 3.8935$ and $n = 4$, $k_\Phi = 0.4108$).

and nitro rotational barriers are presented in Table 6. Because all bonds and dihedral angles were constrained except in the rotational functional group, these barriers should represent the upper bounds to the rotational barriers in the gas phase. As listed in Table 6, the barrier of nitro group (1) (16.2 kcal/mol) is higher than that of nitro group (2) (12.9 kcal/mol) because the nitro group (2) is connected by only one intramolecular hydrogen bond to the amino group. The magnitude of the barrier of the amino group (23.4 kcal/mol) was higher than those of nitro groups (1) and (2).

The force constants of the dihedral angles (k_Φ) are also shown in Table 4. Most of the potential energy curves of the dihedral angles can be expressed by a single form of the potential function ($n = 2$). However, only nitro group (1) cannot be represented by a single form of the potential function because the strong hydrogen bond operates powerfully on nitro group (1). The strong interaction slightly distorts the potential energy curve at around 0.0−15°. Therefore, we fitted the potential energy curve by using two potential functions, such as $n = 2$ and 4, as shown in Table 4. These two functions can fit the potential energy curve well in the range of 0−360°. The best fitted curve is shown in Figure 5.

C. Molecular Dynamics (MD). ***1. Primary Simulation Cell.*** MD calculations were performed on the primary simulation cell, which is shown in Figure 6. The primary simulation cell consists

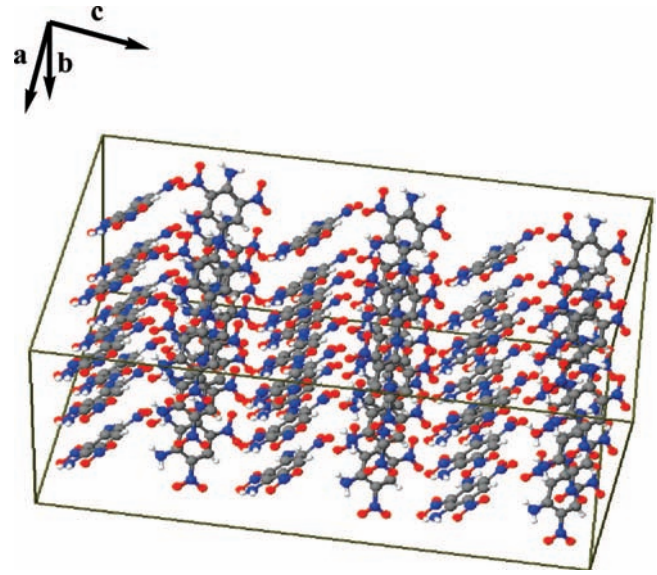

Figure 6. Primary simulation cell. The simulation cell consisted of 54 molecules, which were obtained by replicating the crystallographic unit cell, and contained 27 unit cells (3 × 3 × 3) in a monoclinic cell.

of 54 molecules in a monoclinic cell, which corresponds to 27 unit cells in Figure 2 obtained by X-ray diffraction. The lengths of the box sides were $a = 21.927$ Å, $b = 15.507$ Å, and $c = 34.749$ Å, respectively. In this primary cell, the molecules of DATB are linked together by intermolecular hydrogen bonds into continuous chains along with the *a* axis in the crystal lattice. This hydrogen bond linkage forms a sheetlike structure along the *a* axis. The intermolecular hydrogen bonds exist between O(8′) and H(22) and between O(9′) and H(21). Thereafter, these hydrogen bonds are abbreviated as hydrogen bond (1) and hydrogen bond (2), respectively. It should be pointed out that the *c* axis has no relationship to the intermolecular hydrogen bond network.

2. Pressure Dependence of the Intermolecular Hydrogen Bond Distances. By raising the pressure from 1 atm to 25.0 GPa at every 0.5 GPa, the pressure dependence of the intermolecular hydrogen bond distances in the DATB crystal

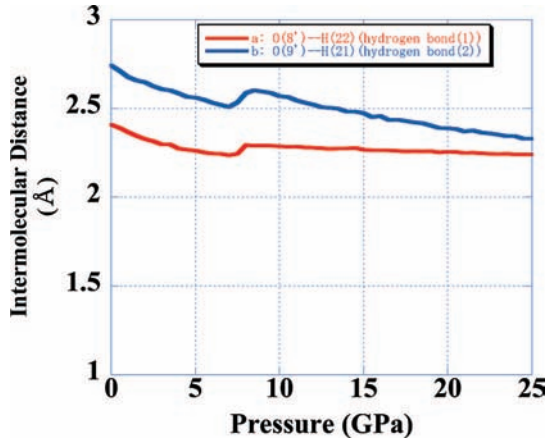

Figure 7. Pressure dependence of intermolecular distances: (a) O(8)−H(22′), hydrogen bond (1); (b) O(9)−H(21′), hydrogen bond (2).

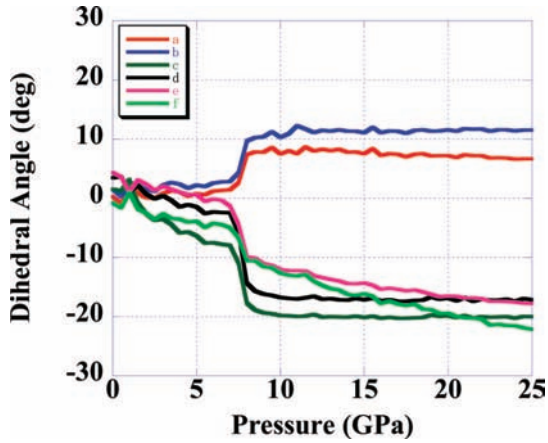

Figure 8. Pressure dependence of dihedral angles of the nitro and amino groups. The dihedral angles were defined by the plane of the nitro or amino group and by the aromatic ring: (a) O14−N13−C1−C6, nitro group (1); (b) O15−N13−C1−C2, nitro group (1); (c) O8−N7−C5−C6, nitro group (2); (d) O9−N7−C5−C4, nitro group (2); (e) H17−N16−C6−C5, amino group; (f) H18−N16−C6−C1, amino group.

were analyzed from the 10 ps time trajectories at every pressure value, as shown in Figure 7. The intermolecular distances of hydrogen bonds (1) and (2) decreased with increasing pressure in the range of 1 atm to 7.0 GPa. However, beginning at 7.5 GPa, the intermolecular distances of both hydrogen bonds increased with the increment in pressure, up to 8.5 GPa, above which the distances again decreased until we reached the maximum pressure of 25.0 GPa in our investigation of this work. This behavior is quite unique because the intermolecular distances should generally monotonously decrease when the pressure increases. To investigate the origin of this change, the behaviors of the dihedral angles of the nitro and amino groups concerning these intermolecular hydrogen bonds were analyzed at different pressures.

3. Pressure Dependence of the Dihedral Angles of Nitro and Amino Groups. Figure 8 shows the pressure dependence of the dihedral angles of the nitro and amino groups. The dihedral angles were defined by the plane of the nitro or amino group and by the aromatic ring concerning hydrogen bonds. In the pressure range of 1 atm to 7.0 GPa, the dihedral angles of the nitro group (1) did not change but stayed around the original position of zero because the nitro group (1) adjoins two amino groups. Therefore, the dihedral angle of the nitro group (1) barely changes with compression under a relatively low pressure

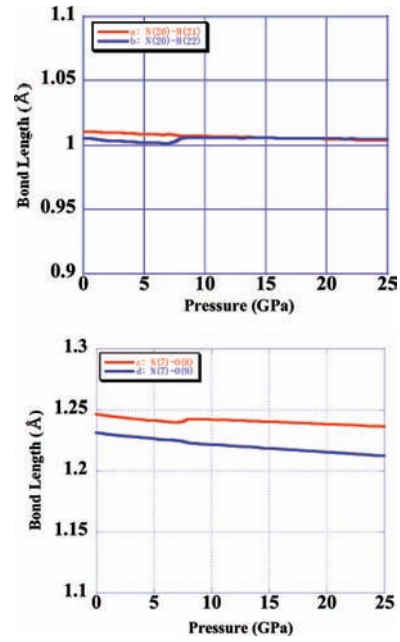

Figure 9. Pressure dependence of bond distances connected to intermolecular hydrogen bonds (a) N(20)−H(21) and N(20)−H(22) and (b) N(7)−O(8) and N(7)−O(9).

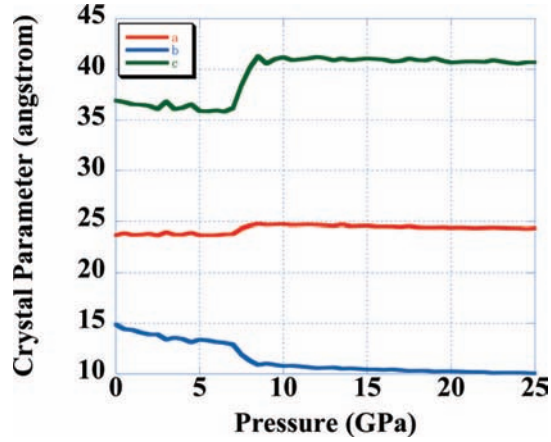

Figure 10. Pressure dependence of cell parameters: (a) *a* axis, (b) *b* axis, and (c) *c* axis.

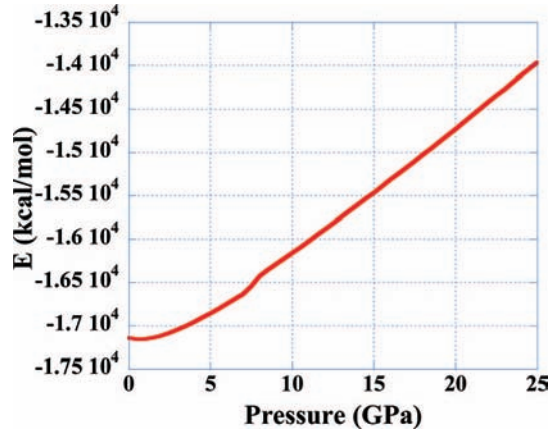

Figure 11. Pressure dependence of total energy.

range. However, the dihedral angle of the two nitro groups (2) became gradually distorted from the planar conformation of this molecule under the same conditions. This may also be explained by the fact that nitro group (2) adjoins only one amino group

TABLE 2: Calculated and Experimental DATB Values

experimental values		calculated values	
	in the crystal	B3LYP/ 6-311++ G(2df,2pd)	B3LYP/ 6-31G(d,p)
Bond Lengths (Å)		Bond Lengths (Å)	
C1−C2	1.442(3)	1.443	1.450
C2−C3	1.439(3)	1.436	1.443
C3−C4	1.369(3)	1.374	1.381
C1−N13	1.430(3)	1.437	1.439
C2−N20	1.321(3)	1.325	1.329
C3−N10	1.449(3)	1.455	1.456
N13−O15	1.238(3)	1.237	1.248
N10−O12	1.243(3)	1.239	1.229
N10−O11	1.225(3)	1.219	1.250
N20−H22	0.91(4)	1.009	1.016
C4−H19	0.93(3)	1.078	1.082
Intramolecular Hydrogen Bond Distances (Å)			
O15−H22	1.79(3)	1.770	1.765
O12−H21	1.88(2)	1.801	1.795
Bond Angles (deg)		Bond Angles (deg)	
C2−C1−C6	123.0(2)	122.0	122.0
C1−C2−C3	116.3(2)	116.7	116.8
C3−C4−C5	121.9(2)	122.3	122.3
O14−N13−O15	118.9(2)	119.9	119.6
O15−N13−C1	120.4(2)	120.0	120.2
C2−N20−H22	115(2)	117.7	117.8
H21−N20−H22	129(3)	124.6	125.7
N13−C1−C2	118.6(2)	119.0	119.0
N20−C2−C1	123.2(2)	123.0	122.9
Dihedrals	Dihedrals Angles (deg)	Dihedrals Angles (deg)	
H17−N16−C6−C5	−5(2)	0.000	0.000
H18−N16−C6−C1	−1(2)	0.000	0.000
H21−N20−C2−C3	4(2)	0.000	0.000
H22−N20−C2−C1	−3(2)	0.000	0.000
O8−N7−C5−C6	4.9(3)	0.000	0.000
O9−N7−C5−C4	4.4(3)	0.000	0.000
O11−N10−C3−C4	−4.9(3)	0.000	0.000
O12−N10−C3−C2	−4.1(3)	0.000	0.000
O14−N13−C1−C6	1.5(3)	0.000	0.000
O15−N13−C1−C2	2.6(3)	0.000	0.000

and by the fact that the resistance to keep the planarity of the molecular plane is not very strong. The amino group also rotated together in the same manner as that of nitro group (2). However, when the pressure reached ~7.5 GPa, all of these dihedral angles suddenly changed. Two dihedral angles of two nitro groups (2) turned around from −3 to −15° and from −8 to −20°, respectively. Furthermore, two dihedral angles of nitro group (1) turned around from 2 to 8° and from 3 to 10°, respectively. This behavior corresponds to the increment of the intermolecular distances of hydrogen bonds that is observed in the range of 7.5 to 8.5 GPa, as discussed in the above section. Therefore, when the intermolecular distances of hydrogen bonds become considerably short with compression under this relatively high pressure range, the total energy of the DATB crystal system will become considerably unstable by the increment of the exchange repulsive force. Under these circumstances, to maintain adequate intermolecular distances of hydrogen bonds, each substituent group related to the hydrogen bonds may be rotated to avoid the increment of the exchange repulsive force.

These abrupt dihedral changes occurred almost simultaneously in all nitro (1), nitro (2), and amino groups, but after we closely examined the MD time courses of the movement of these dihedral angles, we observed that the abrupt change in the dihedral angles occurred not simultaneously but sequentially in the order of the amino group, nitro group (2), and nitro group (1). These results led us to speculate about the beginning process of the DATB decomposition reactions. That is, the stimuli exerted from the external circumstance may be relaxed by the rearrangement of the molecular structure, especially concerning the hydrogen bond moieties. More detailed analysis for this result is in progress.

When pressure exceeded 8.5 GPa, the nitro group (1) and nitro group (2) maintained dihedral angles of about 8.0 to 10.0 and −18.0 to −20.0°, respectively. However, the dihedral angle of the amino group again gradually increased up to about −18.0 to −20.0° at 25.0 GPa. These discrepancies may be attributed to the fact that the magnitude of the amino group's energy barrier is higher than those of the nitro groups (Table 6). The amino group's high-energy barrier comes from the change in the electronic state during the change in the dihedral angle. That is, the electronic state of the amino group gradually transfers from sp^2- to sp^3-like orbital according to the increment of the dihedral angles. Such a change in the electronic state requires high energy, and this may allow the resistance to the dihedral change from the external pressure.

4. Pressure Dependence of the Bond Lengths Related to the Hydrogen Bond. The pressure dependence of the bond lengths of N−O and N−H, which relate to the hydrogen bond, was analyzed, and the results are shown in Figure 9. A similar abrupt change in the bond lengths was also found around 7.5 GPa. At 7.5 GPa, one of the bond lengths of the N−O and one of N−H were slightly elongated, although the N−O and N−H bond lengths gradually decrease in all pressure regions. These abrupt changes of the N−O and N−H bond lengths completely correspond to not only the change in the hydrogen bond-related dihedral angles of the nitro and the amino groups but also the intermolecular hydrogen bond distances discussed above. In our previous experimental results for DATB Raman spectra, there was a turning point in the pressure dependence of the Raman spectra at around 5.0 GPa. We interpreted this to be a change in the hydrogen bond structure.[26] These experimental results are in good agreement with our calculation results shown here.

5. Pressure Dependence of the Crystal Parameters and Total Energy. We calculated the pressure dependence of the crystal parameters by increasing the pressure in increments of 0.5 GPa, as shown in Figure 10. It was found that the lattice parameter of only the *a* axis, which has the same direction as that of the intermolecular hydrogen bond networks, hardly changed with compression. When the pressure increased to 7.5 GPa, the lattice parameters of the *c* axis suddenly elongated by about 5 Å, and inversely, those of the *b* axis shortened by about 2 Å. To investigate the energy changes in these structures, we analyzed the pressure dependence of the total energy, and the results are shown in Figure 11. The total energy gradually increases as the pressure increases up to 7.0 GPa. However, an abrupt increment occurs in the range of 7.5 to 8.5 GPa. Then, as the pressure increases from 9.0 to 25.0 GPa, the total energy again returns to a gradual increment. These results again indicate that the transition point in the DATB crystal is around 7.5 GPa. This point corresponds to the structural turning point with compression discussed above.

To validate the L-J potential at high pressures, the pressure dependence of the crystal parameters and the intermolecular distance of hydrogen bonds in DATB were also calculated by decreasing the pressure from 25 GPa to 1 atm. The change point

TABLE 3: Calculated and Experimental Vibrational Frequencies of DATB

mode no.	assignment	calcd[a]	experimental data[b] IR	experimental data[b] Raman
1	NO_2 twisting out of plane	32.5		
2	NO_2 twisting + N−H twisting out of plane	41.2		
3	ring def. + NO_2 twisting out of plane	46.1		
4	ring def. out of plane	84.9		
5	ring def. out of plane	90.1		123
6	ring def. out of plane	135.8		165
7	NO_2(2) rocking in plane	191.6		210
8	NO_2(1) rocking in plane	252.3		269
9	ring def. out of plane	275.8		286
10	ring def. + NO_2(2) wagging out of plane	309.5		331
11	ring def. + NO_2 rocking in plane	326.1		353
12	ring def. + N−H rocking in plane	343.6		360
13	NO_2 rocking + N−H rocking in plane	365.5		376
14	ring def. + NO_2(2) rocking in plane	368.5		392
15	N−H rocking + ring def. in plane	429.6		445
16	ring def. + N−H rocking + NO_2 rocking in plane	429.7		
17	ring def. + N−H twisting out of plane	450.5		458
18	ring def. + NO_2 rocking + C−H def. in plane	469.8		484
19	ring def. + NO_2(2) rocking + N−H rocking in plane	495.9		514
20	N−H def. wagging out of plane (different direction)	597.9		
21	N−H def. wagging out of plane (same direction)	602.0		
22	ring def. twisting + N−H wagging + NO_2(2) wagging out of plane	654.0		631
23	ring def. + N−H rocking + NO_2(2) scissors + NO_2(1) rocking in plane	662.1		662
24	ring def. + N−H rocking + NO_2 scissors in plane	663.6	675	677
25	ring def. + N−H wagging + NO_2 wagging out of plane	690.3		709
26	ring def. + N−H rocking + NO_2 scissors in plane	711.1	727	732
27	N−H twisting + NO_2 wagging + C−H bending out of plane	727.2	757	761
28	N−H twisting + NO_2(1) wagging out of plane	744.6		
29	ring def. + NO_2 scissors in plane	761.2	777	778
30	N−H twisting + NO_2 wagging + C−H def. + ring def. out of plane	764.8	781	
31	N−H twisting + NO_2(2) wagging + ring def. out of plane	764.8		
32	ring def. + N−H twisting + NO_2(1) wagging out of plane	771.2		
33	ring sym. str. + NO_2 def. in plane	816.0	831	833
34	ring asym. str. + N−H rocking + NO_2(2) scissors in plane	870.5	890	895
35	N−H def. rocking + NO_2 scissors + ring def. in plane	896.0	906	910
36	C−H(ring) def. out of plane	964.6	950	952
37	C−H(ring) def. + N−H rocking + ring def. in plane	1016.0	1030	1032
38	N−H rocking + ring def. + C−N(1) str. in plane	1037.0	1044	1037
39	ring sym. str. (Kekule) + N−H rocking +C−N str. in plane	1123.0		
40	C−H(ring) def. + ring def. + N−H rocking + C−N(1) def. in plane	1152.0		1155
41	C−H(ring) def. + N−H rocking + C−N(1) def. in plane	1230.0		
42	ring sym. str. + NO_2(2) sym. str. + N−H def. in plane	1230.0	1160	1162
43	ring asym. str. + NO_2(2) scissors + N−H bending in plane	1241.0	1210	1218
44	NO_2 scissors + N−H bending + C−N str. in plane	1280.0	1255	1260
45	ring asym. str. + N−H bending + NO_2(1) asym. str. in plane	1325.0		
46	ring sym. str. + N−H rocking + NO_2(2) asym. str. in plane	1354.0	1302	
47	ring asym. str. + N−H bending + NO_2 asym. str. in plane	1354.0		1309
48	N−H scissors + ring sym. str. + NO_2(2) asym. str. + NO_2(1) scissors + C−N str. in plane	1414.0	1377	1375
49	ring sym. str. + N−H bending + NO_2(2) asym. str. in plane	1462.0		1424
50	ring asym. str. + NO_2 asym. str. + N−H scissors in plane	1470.0		1469
51	NO_2(1) asym. str. + ring asym. str. + C−H bend. + C−N(H) str. in plane	1506.0	1474	1485
52	N−H def. bending + NO_2 asym. str. + ring def. in plane	1531.0	1524	1527
53	N−H scissors + NO_2(2) asym. str. + ring. def. in plane	1534.0		
54	ring sym. str. + N−H bending + NO_2(2) asym. str. in plane	1566.0	1558	1579
55	ring asym. str. + NO_2 asym. str. + N−H bend. in plane	1588.0	1603	1609
56	C−H (ring) stretching	3121.0	3092	3097
57	N−H sym. str. (not synchronized)	3334.0	3282	
58	N−H sym. str. (synchronized)	3334.0		3289
59	N−H asym. str. (not synchronized)	3452.0	3388	3398
60	N−H asym. str. (synchronized)	3461.0		

[a] B3LYP/6-311G++(2df,2pd) level of theory. [b] ref 27.

was found to correspond to the structural turning point with compression. Therefore, the L-J potential would be useful under high pressure of up to 25.0 GPa. All of these findings together suggest the importance of hydrogen bonds in the impact (pressure)-induced decomposition of the DATB crystal. When a stimulus is exerted by external circumstances, its energy may be absorbed by the rearrangement of the molecular structure of the hydrogen bond moieties. These hydrogen-bonding networks may work as a safety circuit to reduce the sensitivity. When a strong external stimulus is exerted on the crystal, the intermo-

TABLE 4: Force Constants of DATB at the B3LYP/6-31G(d,p) level

bond	k_b (kcal/(mol·Å^2))	l_0 (Å)[a]	bond	k_b (kcal/(mol·Å^2))	l_0 (Å)[a]
C1−C2	358.47	1.4502	N16−H18	501.32	1.0163
C1−C6	357.47	1.4502	C2−N20	486.98	1.3289
C2−C3	354.17	1.4425	N20−H21	501.57	1.0191
C6−C5	354.17	1.4425	N20−H22	501.32	1.0163
C3−C4	434.70	1.3811	C5−N7	274.91	1.4556
C4−C5	434.70	1.3811	N7−O8	575.86	1.2498
C1−N13	256.37	1.4390	N7−O9	562.42	1.2286
N13−O14	561.82	1.2480	C3−N10	274.91	1.4556
N13−O15	561.82	1.2480	N10−O11	575.86	1.2498
C6−N16	486.98	1.3289	N10−O12	562.42	1.2286
N16−H17	501.57	1.0191	C4−H19	358.63	1.0819

bond angle	k_θ (kcal/(mol·rad^2))	θ_0 (deg)[b]	bond angle	k_θ (kcal/(mol·rad^2))	θ_0 (deg)[b]
O14−N13−O15	171.55	119.6198	C2−C3−N10	179.71	122.9368
O14−N13−C1	143.7	120.1896	C5−N7−O8	145.69	119.3541
O15−N13−C1	143.7	120.1896	O8−N7−O9	167.47	122.4741
N13−C1−C6	206.15	119.0232	C5−N7−O9	145.69	119.3541
N13−C1−C2	206.15	119.0232	C3−N10−O11	145.69	119.3541
C1−C6−N16	139.69	122.9404	O11−N10−O12	167.47	122.4741
C1−C2−N20	139.69	122.9404	C3−N10−O12	145.69	119.3541
C6−N16−H18	61.33	117.7976	C4−C5−N7	168.83	115.9762
C6−N16−H17	61.33	117.7976	C5−C4−H19	63.11	118.8495
H17−N16−H18	45.66	125.6607	C4−C3−N10	168.83	115.9762
C2−N20−H22	61.33	117.7976	C3−C4−H19	63.11	118.8495
C2−N20−H21	61.33	117.7976	C2−C1−C6	190.45	121.9622
H21−N20−H22	45.66	125.6607	C1−C2−C3	188.98	116.7715
N16−C6−C5	145.34	120.2900	C2−C3−C4	177.22	121.0932
N20−C2−C3	145.34	120.2900	C3−C4−C5	169.04	122.3162
C6−C5−N7	179.71	122.9368	C4−C5−C6	177.22	121.0932
C1−C6−C5	188.98	116.7715			

dihedral angle	k_Φ (kcal/(mol·rad^2))	n	δ (deg)	dihedral angle	k_Φ (kcal/(mol·rad^2))	n	δ (deg)
H17−N16−C6-C1	3.6748	2	180	O11−N10−C3-C2	2.5095	2	180
H17−N16−C6-C5	3.6748	2	180	O11−N10−C3-C4	2.5095	2	180
H18−N16−C6-C1	3.6748	2	180	O12−N10−C3-C2	2.5095	2	180
H18−N16−C6-C5	3.6748	2	180	O12−N10−C3-C4	2.5095	2	180
H21−N20−C2-C1	3.6748	2	180	O14−N13−C1-C2	3.8935	2	180
H21−N20−C2-C3	3.6748	2	180	O14−N13−C1-C2	0.4108	4	180
H22−N20−C2-C1	3.6748	2	180	O14−N13−C1-C6	3.8935	2	180
H22−N20−C2-C3	3.6747	2	180	O14−N13−C1-C6	0.4108	4	180
O8−N7−C5-C4	2.5095	2	180	O15−N13−C1-C2	3.8935	2	180
O8−N7−C5-C6	2.5095	2	180	O15−N13−C1-C2	0.4108	4	180
O9−N7−C5-C4	2.5095	2	180	O15−N13−C1-C6	3.8935	2	180
O9−N7−C5-C6	2.5095	2	180	O15−N13−C1-C6	0.4108	4	180

[a] Equilibrium value. [b] Equilibrium value.

lecular distances of hydrogen bonds increase to stabilize the molecule in the crystalline state. These hydrogen-bonding networks may play an important role as a "molecular stabilizer" in energetic materials. The practical pressure of an ordinary booster to initiate secondary explosives is estimated to be up to 20−30 GPa. This stimulus is the same order as the pressure range around the transition range found in this work. Without the above hydrogen-bonding networks in the DATB crystal, the crystal would explode, even in a weak stimulus of <20 GPa.

5. Conclusions

In the area of nitro aromatic explosives, a number of studies have been carried out to support the idea that the C-NO_2 bond is a key to determining the shock sensitivity.[27] From these studies, it has been noted that the increment in the number of amino group substitutions in the molecule decreases the sensitivity of nitro aromatic explosives.[28–30] In view of the electronic theory of organic chemistry, the electronic density of the C−NO_2 bond increases by the substitution of strongly electron-donating groups, such as $-NH_2$.[31,32] This is a widely accepted explanation of why the sensitivity of nitro aromatic explosives decreases with the increment of the C−NO_2 bond strength introduced by the electron donation. This explanation seems to be rational when we consider the mechanism underlying the sensitivity of an isolated molecule. However, we also have data showing that the crystal polymorphism would affect the sensitivity of the explosive molecules. This phenomenon cannot be explained when we consider the properties of only the isolated molecule. In the actual explosion process, external high pressure is exerted on a crystal structure of explosives. This indicates the necessity of the study not only for the isolated molecule but also for the crystal system.

In the present work, MD calculations were performed to reveal the effect of high pressure on DATB in the crystalline state. The pressure dependence of the intermolecular distance of hydrogen bonds in DATB was calculated by increasing the pressure up to 25.0 GPa. A unique structural change in DATB crystal was found around 7.5 GPa. The intermolecular distance begins to increase at 7.5 GPa and keeps increasing to 8.5 GPa.

TABLE 5: Electrostatic Charges for DATB Molecule Determined by Merz−Kollman−Singh Procedure at the B3LYP/6-31G(d,p) Level

atom	charge (|e|)
C1	–0.4593
C2	0.5159
C3	–0.2363
C4	–0.0563
C5	–0.2503
C6	0.5410
N7	0.7270
O8	–0.4558
O9	–0.3803
N10	0.7220
O11	–0.3795
O12	–0.4537
N13	0.8135
O14	–0.4605
O15	–0.4607
N16	–0.9055
H17	0.4708
H18	0.4773
H19	0.1775
N20	–0.8834
H21	0.4631
H22	0.4733

TABLE 6: Calculated Rotational Barrier of the Amino and Nitro Groups in DATB Molecule at the B3LYP/6-31G(d,p) Level

group	rotational barrier (kcal/mol)
nitro group (1)	16.2
nitro group (2)	12.9
amino group	23.4

The changes in the dihedral angles of nitro groups and amino groups of intermolecular hydrogen bonds under pressure were analyzed, and these results proved that intermolecular distances increased in proportion to the change in the dihedral angle. By analyzing the pressure dependence of the crystal parameter, we found that the distance of only the *a* axis in the direction of intermolecular hydrogen bonds hardly changed. Also, it was proved that the hydrogen bond plays an important role in stabilizing the whole energy of the crystal system. These inter- and intramolecular hydrogen-bonding networks may play important roles in the "safety circuit" in energetic materials. These results of the MD calculations are in good agreement with our experimental data. Experimental works to obtain detailed information about the relationship between these data under high pressure and the insensitive property of the DATB crystal are in progress and will be published in the near future.

Acknowledgment. The DFT computations were performed using the Research Center for Computational Science, Okazaki, Japan, in particular, a Fujitsu VPP5000 and PRIMEQUEST. We also thank Prof. Tohru Koike of the National Defense Academy and Prof. Yoshiaki Hidaka of Ehime University for his deep consideration of, and helpful advice on, this work.

Supporting Information Available: X-ray crystallographic file of (CIF) DATB. This material is available free of charge via the Internet at http://pubs.acs.org.

References and Notes

(1) Meyer, R.; Köhler, J.; Homburg, A. *Explosives*, 5th ed.; Wiley-VCH: Weinheim, Germany, 2002.
(2) Hiyoshi, R. I.; Kohno, Y.; Takahashi, O.; Nakamura, J.; Yamaguchi, Y.; Matsumoto, S.; Azuma, N.; Ueda, K. *J. Phys. Chem. A* **2006**, *110*, 9816–9827.
(3) Brill, T. B.; James, K. J. *J. Phys. Chem.* **1993**, *97*, 8752–8758.
(4) Rogers, J. W., Jr.; Peebles, H. C.; Rye, R. R.; Houston, J. E.; Binkley, J. S. *J. Chem. Phys.* **1984**, *80*, 4513–4520.
(5) Wu, C. J.; Fried, L. E. *J. Phys. Chem. A* **2000**, *104*, 6447–6452.
(6) Pravica, M.; Yulga, B.; Liu, Z.; Tschauner, O. *Phys. Rev. B* **2007**, *76*, 064102.
(7) Baldridge, K. K.; Siegel, J. S. *J. Am. Chem. Soc.* **1993**, *115*, 10782–10785.
(8) Kunz, A. B. *Phys. Rev. B* **1996**, *53*, 9733–9738.
(9) Manaa, M. R.; Gee, R. H.; Fried, L. E. *J. Phys. Chem. A* **2002**, *106*, 8806–8810.
(10) Manaa, M. R.; Fried, L. E.; Reed, E. J. *J. Comput.-Aided Mater. Design* **2003**, *10*, 75–97.
(11) Wu, C. J.; Yang, L. H.; Fred, L. E.; Quenneville, J.; Martinez, T. J. *Phys. Rev. B* **2003**, *67*, 235101.
(12) Gee, R. H.; Roszak, S.; Balasubramanian, K.; Fried, L. E. *J. Chem. Phys.* **2004**, *120*, 7059–7066.
(13) Huang, Z.; Chen, B.; Gao, G. *J. Mol. Struct.* **2005**, *87*, 752–792.
(14) Tu, Y.; Luo, Y.; Agren, H. *J. Phys. Chem. B* **2005**, *109*, 16730–16735.
(15) Liu, H.; Zhao, J.; Ji, G.; Wei, D.; Gong, Z. *Phys. Lett. A* **2006**, *358*, 63–69.
(16) Yin, K.; Zou, D.; Zhong, J.; Xu, D. *Comput. Mater. Sci.* **2007**, *38*, 538–542.
(17) Liu, H.; Zhao, J.; Du, J.; Gong, Z.; Ji, G.; Wei, D. *Phys. Lett. A* **2007**, *367*, 383–388.
(18) Holden, J. R. *Acta Crystallogr.* **1967**, *22*, 545–550.
(19) SIR92: Altomare, A.; Burla, M.; Camalli, C. M.; Cascarano, M.; Giacovazzo, C.; Guagliardi, A.; Polidori, G. *J. Appl. Crystallogr.* **1994**, *27*, 435.
(20) DIRDIF94: Beurskens, P. T.; Admiraal, G.; Beurskens, G.; Bosman, W. P.; Gelder, R. de.; Israel, R.; Smits, J. M. M. *The DIRDIF-94 Program System*; Technical Report of the Crystallography Laboratory; University of Nijmegen: The Netherlands, 1994.
(21) teXsan: *Crystal Structure Analysis Package*; Molecular Structure Corporation: The Woodlands, TX, 1985 and 2004.
(22) Brooks, B. R.; Bruccoleri, R. E.; Olafson, B. D.; States, D. J.; Swaminathan, S.; Karplus, M. *J. Comput. Chem.* **1983**, *4*, 187–217.
(23) Frisch, M. J.; Trucks, G. W.; Schlegel, H. B.; Scuseria, G. E.; Robb, M. A.; Cheeseman, J. R.; Zakrzewski, V. G.; Montgomery, J. A.; Stratmann, Jr., R. E.; Burant, J. C.; Dapprich, S.; Millam, J. M.; Daniels, A. D.; Kudin, K. N.; Strain, M. C.; Farkas, O.; Tomasi, J.; Barone, V.; Cossi, M.; Cammi, R.; Mennucci, B.; Pomelli, C.; Adamo, C.; Clifford, S.; Ochterski, J.; Petersson, G. A.; Ayala, P. Y.; Cui, Q.; Morokuma, K.; Salvador, P.; Dannenberg, J. J.; Malick, D. K.; Rabuck, A. D.; Raghavachari, K.; Foresman, J. B.; Cioslowski, J.; Ortiz, J. V.; Baboul, G.; Stefanov, B. B.; Liu, G.; Liashenko, A.; Piskorz, P.; Komaromi, I.; Gomperts, R.; Martin, R. L.; Fox, D. J.; Keith, T.; Al-Laham, M. A.; Peng, C. Y.; Nanayakkara, A.; Challacombe, M.; Gill, P. M. W.; Johnson, B.; Chen, W.; Wong, M. W.; Andres, J. L.; Gonzalez, C.; Head-Gordon, M.; Replogle, E. S.; Pople, J. A. *Gaussian 98*, revision A.11.1; Gaussian, Inc.: Pittsburgh, PA, 2001.
(24) Forseman, J. B., Frisch, A. *Exploring Chemistry with Electronic Structure Methods*, 2nd ed.; Gaussian, Inc.: Pittsburgh, PA, 1996.
(25) The diagram was drawn using Mercury 1.4.2 (http://www.ccdc.cam.ac.uk/mercury/).
(26) Hiyoshi, R. I.; Kohno, Y.; Nakamura, J.; Ueda, K. In *Proceedings of the 13th International Detonation Symposium*, Norfolk, VA, 2006; pp 1007−1015.
(27) Murray, J. S.; Lane, P.; Politzer, P.; Bolduc, P. R. *Chem. Phys. Lett.* **1990**, *168* (2), 135–139.
(28) Owens, F. J. *J. Mol. Struct.: THEOCHEM* **1985**, *121*, 213–220.
(29) Kamlet, M. J.; Adolph, H. G. *Propellants, Explos., Pyrotech.* **1979**, *4*, 30–34.
(30) Dodson, B. W.; Graham, R. A. In *Shock Waves in Condensed Materials*; Nellis, W. J., Seaman, L., Graham, R. A., Eds.; American Institute of Physics: New York, 1982.
(31) Owens, F. J.; Jayasuriya, K.; Abraham, L.; Politzer, P. *Chem. Phys. Lett.* **1985**, *116*, 434–438.
(32) Politzer, P.; Jayasuriya, K.; Sjoberg, P.; Laurence, P. R. *J. Am. Chem. Soc.* **1985**, *107*, 1174–1177.

JP809240X